4 The Foundations of Dynamical Mean-Field Theory

Marcus Kollar
Center for Electronic Correlations and Magnetism,
Institute for Physics
University of Augsburg

Contents

E. Pavarini, E. Koch, A. Lichtenstein, and D. Vollhardt (eds.)
DMFT: From Infinite Dimensions to Real Materials
Modeling and Simulation Vol. 8
Forschungszentrum Jülich, 2018, ISBN 978-3-95806-313-6
http://www.cond-mat.de/events/correl18

1 Introduction

In this Lecture the foundations of dynamical mean-field theory (DMFT) for interacting electrons will be reviewed along the following route. As already described in the Lecture of D. Vollhardt, the first step involves the limit of infinite lattice dimension, $d \to \infty$. We will discuss this limit for fermions in Sec. 2. The resulting scaling of hopping parameters with d then makes the effect of electronic interactions in Hubbard-type models more manageable, as discussed in Sec. 3. Namely, the Feynman diagrams contributing to the Green function in perturbation theory simplify, and as a result the self-energy becomes local, i.e., independent of momentum. The derivation of DMFT is then completed by mapping Hubbard-type models in infinite dimensions to single-site impurity models with a self-consistency condition (Sec. 4), which have the same self-energy but can be solved numerically. Note that other derivations of this last step are available [1–5]. Note also that the present lecture notes draw largely on a previous presentation [6].

The Hubbard model is the simplest model for describing the physics of correlated electrons, i.e., electrons which do not behave independently due to their Coulomb interaction. For a single band it can be written as

$$H = H_0 + H_1 \,, \tag{1a}$$

$$H_0 = \sum_{ij\sigma} t_{ij}\, c^\dagger_{i\sigma} c_{j\sigma} = \sum_{\boldsymbol{k}\sigma} \varepsilon_{\boldsymbol{k}}\, c^\dagger_{\boldsymbol{k}\sigma} c_{\boldsymbol{k}\sigma} \,, \tag{1b}$$

$$H_1 = U \sum_i n_{i\uparrow} n_{i\downarrow} \,, \tag{1c}$$

where t_{ij} is the hopping amplitude from site i to j, and the dispersion relation $\varepsilon_{\boldsymbol{k}}$ is its Fourier transform; for our purposes we will assume a tight-binding form. For each doubly occupied site the Hubbard interaction U is contributed to the energy of a state. To describe the electronic structure of correlated materials, more complicated models and methods are typically needed, e.g., involving several bands as obtained from density functional theory, including more complicated on-site interactions, taking retardation effects into account, reconciling a calculated charge distribution with the model parameters determined by it, nonlocal and nonequilibrium effects, and so on. For these topics we refer to the other Lectures in this book. In these contexts, as well as for (1), the goal and spirit of DMFT is to provide a controlled starting point for a reliable treatment of interactions and the induced electronic correlations.

2 Fermions in the limit of infinite lattice dimension

We begin with the limit of infinite spatial dimensions, $d \to \infty$, as introduced in Ref. [7]. First the three-dimensional simple cubic lattice is generalized to the d-dimensional hypercubic lattice in order to obtain the corresponding tight-binding dispersion for nearest-neighbor hopping. The

hypercubic lattice simply has the unit cell basis vectors

$$\begin{aligned} \boldsymbol{e}_1 &= (1,0,0,\ldots,0)\,, \\ \boldsymbol{e}_2 &= (0,1,0,\ldots,0)\,, \\ &\ldots \\ \boldsymbol{e}_d &= (0,0,0,\ldots,1)\,. \end{aligned} \tag{2}$$

A nearest-neighbor hopping amplitude t_{ij} and corresponding dispersion then have the form

$$t_{ij} = t(\boldsymbol{R}_i - \boldsymbol{R}_j) = \begin{cases} -t & \text{if } \boldsymbol{R}_i - \boldsymbol{R}_j = \pm \boldsymbol{e}_n\,, \\ 0 & \text{otherwise}\,, \end{cases} \tag{3}$$

$$\varepsilon_{\boldsymbol{k}} = -2t \sum_{i=1}^{d} \cos k_i\,. \tag{4}$$

We will proceed in two ways to obtain the corresponding density of states (L: number of lattice sites)

$$\rho(\omega) = \frac{1}{L} \sum_{\boldsymbol{k}} \delta(\omega - \varepsilon_{\boldsymbol{k}})\,. \tag{5}$$

A succinct technique is to employ the central limit theorem for probability distributions [7]. One defines random variables $X_i = \sqrt{2}\cos k_i$ in terms of independent random variables k_i, which are independently and uniformly distributed in the interval $[-\pi, \pi]$. Since X_i has zero mean and unit variance, the random variable $X_d = \frac{1}{\sqrt{d}} \sum_{i=1}^{d} X_i$ converges in law to a normal distributed random variable X, again with zero mean and unit variance. Here convergence in law means that the distribution function of X_d converges to the normal distribution $\exp(-x^2/2)/\sqrt{2\pi}$. If we then consider the density of states $\rho(\varepsilon)$ as the distribution function of the random variable $\sqrt{2d}\,t\,X_d$, we see that a finite density of states is obtained only if we scale the hopping amplitude is proportional to $d^{-1/2}$ for $d \to \infty$. We thus have, replacing the sum over the first Brillouin zone in (5) by an integral in the thermodynamic limit,

$$\rho(\varepsilon) = \int \frac{d^d k}{(2\pi)^d}\, \delta(\varepsilon - \varepsilon_{\boldsymbol{k}}) = \frac{1}{2\pi |t_*|}\, \exp\left[-\frac{\varepsilon^2}{2t_*^2}\right] \qquad \text{for } \; t = \frac{t_*}{\sqrt{2d}}\,, \tag{6}$$

where t_* is independent of d. We thus obtain a Gaussian density of states with finite variance, and hence also a finite kinetic energy per lattice site. With the scaling $t \propto 1/\sqrt{d}$ the kinetic energy and the Hubbard interaction energy thus remain of the same order of magnitude in the limit $d \to \infty$ and hence in competition with each other. Fig. 1 depicts several densities of states for different d, showing the approach to a Gaussian for large d.

Alternatively, one can follow the idea of the proof of the central limit theorem, which uses Fourier transforms of probability distributions. We thus consider the Fourier transform of

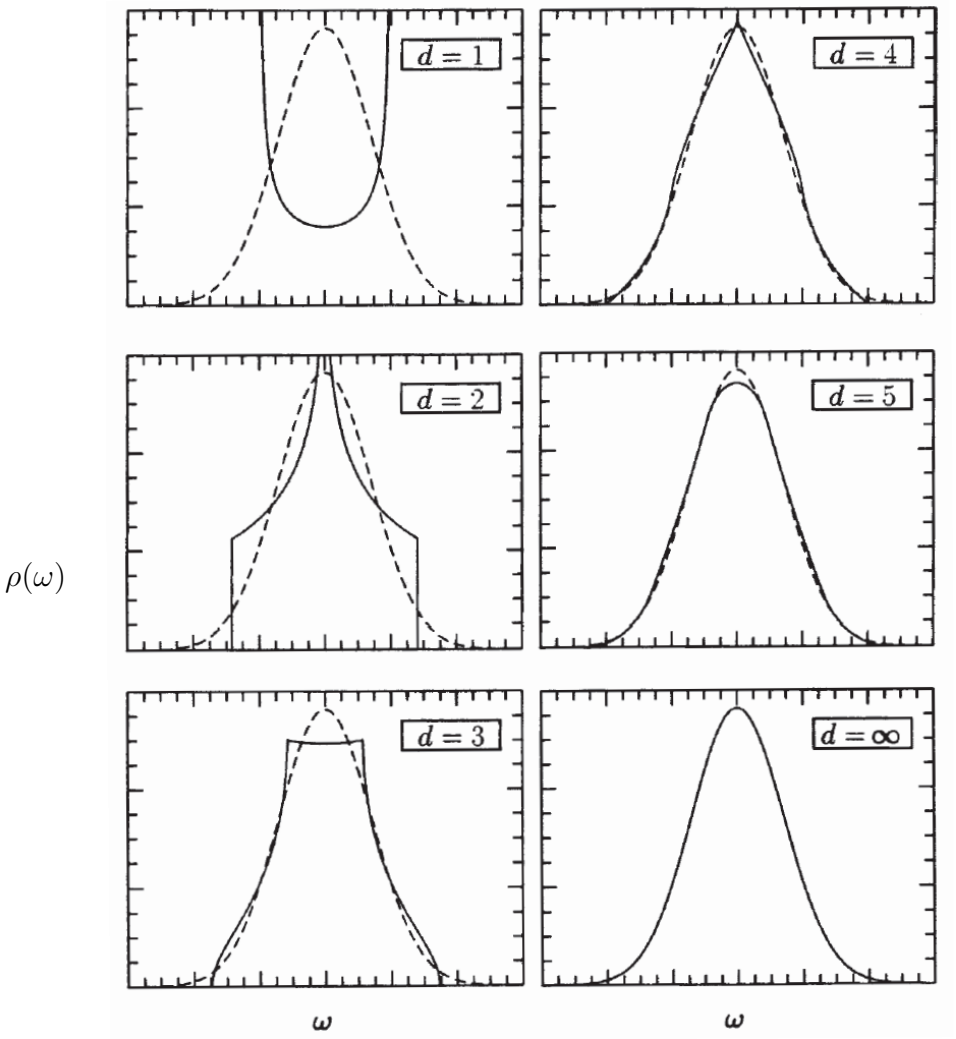

Fig. 1: *Density of states for hopping on hypercubic lattice for several d, compared to the Gaussian that is obtained in $d \to \infty$. From Ref. [2].*

$\rho(\varepsilon)$ [8], which separates into independent factors for each dimension,

$$\Phi(s) = \int_{-\infty}^{\infty} d\varepsilon \; e^{is\varepsilon} \; \rho(\varepsilon) = \int \frac{d^d k}{(2\pi)^d} \; e^{is\varepsilon_{\boldsymbol{k}}} = \left[\int_{-\pi}^{\pi} \frac{dk}{2\pi} \; \exp\left(-\frac{2ist_*}{\sqrt{2d}} \; \cos k \right) \right]^d$$

$$= J_0\left(\frac{2st_*}{\sqrt{2d}} \right)^d = \left[1 - \frac{t_*^2 s^2}{2d} + \mathcal{O}\left(\frac{1}{d^2} \right) \right]^d = \exp\left[-\frac{t_*^2 s^2}{2} + \mathcal{O}\left(\frac{1}{d} \right) \right]. \tag{7}$$

Here $J_0(z)$ is a Bessel function, which has been Taylor expanded, integrated, and reexponentiated. Performing the inverse transform yields

$$\rho(\varepsilon) = \int_{-\infty}^{\infty} \frac{d\varepsilon}{2\pi} \; e^{-is\varepsilon} \; \Phi(s) = \frac{1}{2\pi |t_*|} \; \exp\left[-\frac{\varepsilon^2}{2t_*^2} + \mathcal{O}\left(\frac{1}{d} \right) \right], \tag{8}$$

By keeping more terms in the Taylor expansion of the Bessel function one can derive further terms in an asymptotic series in powers of $1/d$ [8].

We conclude that the nearest-neighbor hopping amplitude must be scaled with $1/\sqrt{d}$ to obtain a meaningful large-dimensional limit. More generally, each hopping amplitude t_n must be scaled proportional to $1/\sqrt{Z_n}$, where the coordination number Z_n denotes the number of sites which are connected to a given site by t_n, e.g., $Z_1 = 2d$ for nearest-neighbor hopping and $Z_2 = (2d-1)2d = (Z-1)Z$ for next-nearest-neighbor hopping on the hypercubic lattice, and so on. The density of states for a more complicated hopping matrix can also be obtained. For example, for nearest-neighbor and next-nearest-neighbor hopping a singularity develops at one of the band edges [9]. A general mapping can be constructed between the hopping matrix on the hypercubic lattice and its density of states [10, 11], which also to determine the hopping amplitudes for a given density of states.

A conceptual and practical drawback of a Gaussian density of states is that it extends up to infinite positive and negative energies ε. For other generalized lattices, such as the face-centered-hypercubic lattice [12] (which is asymmetric and has one finite band edge) or the hyperdiamond lattice [13] (for which the symmetric density of states vanishes at $\varepsilon = 0$), the bandwith is also infinite. One of the few lattices with finite bandwidth for nearest-neighbor hopping is the Bethe lattice, i.e., an infinite Cayley tree of which each node has Z nearest neighbors. This recursively defined lattice (which is not a periodic crystal lattice) has a semi-elliptic density of states with a finite bandwidth in the limit $Z \to \infty$ for scaled nearest-neighbor hopping $t = t_*/\sqrt{Z}$,

$$\rho_{\text{Bethe}}(\varepsilon) = \begin{cases} \dfrac{\sqrt{4t_*^2 - \varepsilon^2}}{2\pi t_*^2} & \text{for } |\varepsilon| \leq 2|t_*| \\ 0 & \text{otherwise} \end{cases} . \tag{9}$$

For comparison, for finite coordination number Z, the density of states reads $\rho_{\text{Bethe},Z}(\varepsilon) = \rho_{\text{Bethe}}(\varepsilon) \;/\; [\frac{Z}{Z-1} - \frac{\varepsilon^2}{t_*/\sqrt{Z-1}}]$. These results can be obtained, e.g., with recursive methods (see Refs. [14, 15] and references therein), which can also be used to find the density of states for longer-range hopping or to construct a set of hopping parameters yielding a given density of states.

It is rather typical for tight-binding dipersions in infinite dimensions to lead to one or both band edges at infinite energy. This is a qualitative difference to a finite-dimensional system which always has finite band edges for finite hopping amplitudes. In practice one therefore regards the simplifications following from the infinite-dimensional limit (discussed below) as independent of the dispersion, and simply uses the density of states of the finite-dimensional system of interest in the calculations. This is justified in particular for single-particle quantities into which only the dispersion $\varepsilon_{\boldsymbol{k}}$ enters in infinite dimensions (but no detailed dependence on $\boldsymbol{k}$). If necessary one can use one of the procedures, i.e., for the hypercubic [10] or Bethe lattice [14], to construct a set of hopping amplitudes that realizes a given density of states of a finite-dimensional lattice. Any density of states with finite bandwidth can be represented in infinite dimensions in this way, although long-ranged hopping amplitudes are typically required.

3 Consequences for many-body theory

The scaling of hopping amplitudes with negative powers of the dimension (or coordination number), discussed in the previous section, leads to simplifications in the many-body theory for Hubbard-type models such as (1). However, these simplifications will not hold at the Hamiltonian level, but rather at the level of Green functions and effective actions. We, therefore, first review some definitions and basic concepts of many-body theory that are essential for the formulation and understanding of DMFT.

3.1 Green function, spectral function, self-energy, quasiparticles

The simplest dynamical quantity which measures the equilibrium properties of a correlated electron system is the electronic Green function [16–18]. A Green function G_{AB} is defined as an expectation value of operators A and B taken at different (real or imaginary) times in a thermal state, i.e., with density matrix $\propto \exp(-\beta(H-\mu N))$ corresponding to the temperature $T=1/\beta$, or possibly the ground state. Hence it measures the probability amplitude for a propagation of a particle or hole excitation in an equilibrium state if A and B are annihilation and creation operators. Note that this involves eigenstates of the Hamiltonian that differ by one in particle number, and which can describe quite different physical states in the presence of interactions.
In finite-temperature problems one uses the imaginary-time-ordered (fermionic) single-particle Green function $G_{\alpha\beta}(\tau)$, i.e., we put $A = c_\alpha$, $B = c^\dagger_\beta$, with α, β being general momentum or site indices, including also spin and orbital quantum numbers. For imaginary-time Heisenberg operators $A(\tau) = e^{H\tau} A e^{-H\tau}$ (so that $A^\dagger(\tau) \neq (A(\tau))^\dagger$), one defines

$$G_{\alpha\beta}(\tau) = -\langle T_\tau c_\alpha(\tau) c^\dagger_\beta(0)\rangle = -\begin{cases} \langle c_\alpha(\tau) c^\dagger_\beta(0)\rangle & \tau > 0 \\ -\langle c^\dagger_\beta(0) c_\alpha(\tau)\rangle & \tau \leq 0 \end{cases} \tag{10a}$$

$$= -G_{\alpha\beta}(\tau+\beta) \quad \text{for } -\beta < \tau < 0. \tag{10b}$$

(Note that in Ref. [17] the prefactor -1 is not part of the definition.) The dependence only on time differences and the anti-periodicity (10b) follow from the cyclic properties of the trace and the fermionic anticommutation relations. The so-called Matsubara Green function $G_{\alpha\beta}(i\omega_n)$ is obtained by Fourier transforming,

$$G_{\alpha\beta}(i\omega_n) = \int_0^\beta d\tau\; G_{\alpha\beta}(\tau)\; e^{i\omega_n \tau}\,, \tag{11}$$

$$G_{\alpha\beta}(\tau) = T \sum_{n=-\infty}^{+\infty} G_{\alpha\beta}(i\omega_n)\; e^{-i\omega_n \tau}\,, \tag{12}$$

with fermionic Matsubara frequencies $i\omega_n = 2\pi T(n+1/2)$. An explicit expression for the Green function can be obtained by inserting the complete set of eigenstates of the Hamiltonian. One then obtains the spectral representation

$$G_{\alpha\beta}(i\omega_n) = \int_{-\infty}^{\infty} d\omega\, \frac{A_{\alpha\beta}(\omega)}{i\omega_n - \omega}, \tag{13}$$

with the spectral function $A_{\alpha\beta}(\omega)$ given by its so-called Lehmann representation as

$$A_{\alpha\beta}(\omega) = \frac{1}{Z}\sum_{n,m}\langle n|c_\beta^\dagger|m\rangle\langle m|c_\alpha|n\rangle\ (e^{-\beta E_m} - e^{-\beta E_n})\ \delta(\omega - (E_n - E_m))\,, \tag{14}$$

where Z is the partition function and E_n eigenvalues and $|n\rangle$ the eigenstates of $H-\mu N$. We note that in particular $A_{\alpha\alpha}(\omega) \geq 0$. In practice the spectral or Green function can be evaluated via the Lehmann representation only for sufficiently small systems, i.e., when the many-body energy eigenvalues and eigenstates can be obtained directly. For a finite system, the spectral function (and Green function) consists of a finite sum of delta functions, but in the thermodynamic limit these functions typically become continuous just like the non-interacting density of states.
The spectral function occurs not only in the finite-temperature Matsubara Green function, but also, e.g., in the retarded Green function,

$$G^{\text{ret}}_{\alpha\beta}(\omega) = \int_{-\infty}^{\infty} d\omega' \frac{A_{\alpha\beta}(\omega')}{\omega + i0^+ - \omega'}\,, \tag{15}$$

which corresponds to a Green function in the time domain that involves real-time Heisenberg operators. From the pole structure it follows that

$$A_{\alpha\beta}(\omega) = -\frac{1}{\pi}\,\text{Im}\ G^{\text{ret}}_{\alpha\beta}(\omega)\,, \tag{16}$$

and that the retarded Green function can be obtained from the Matsubara Green function by analytic continuation from $i\omega_n$ to $\omega + i0^+$. (The advanced Green function, which is not discussed here, corresponds to the replacement of $i\omega_n$ by $\omega - i0^+$) Note that in a Matsubara Green function this replacement may only be done at the very end of a calculation, because the anti-periodicity in imaginary time must typically have been at work first. In view of the spectral representations (13) and (15) on often writes $G_{\alpha\beta}(\omega)$ for both the Matsubara or retarded Green function, with the understanding that the argument is either $i\omega_n$ for the former or $\omega + i0^+$ for the latter, and hence is never purely real.
The indices α, β, ... represent lattice site or momentum $\boldsymbol{k}$, as well as spin index σ (and possibly orbital or band index). The real-space and momentum-space Green functions are related by a Fourier transform. Of particular importance is the local Green function

$$G_{ii\sigma}(\omega) = G_\sigma(\omega) = \frac{1}{L}\sum_{\boldsymbol{k}} G_{\boldsymbol{k}\sigma}(\omega)\,, \tag{17}$$

$$A_{ii\sigma}(\omega) = A_\sigma(\omega) = -\frac{1}{\pi}\,\text{Im}\ G_\sigma(\omega + i0^+)\,, \tag{18}$$

where translational invariance has been assumed, e.g., as in (3).
For non-interacting particles, with Hamiltonian $H_0 - \mu N = \sum_{\boldsymbol{k}\sigma}(\varepsilon_{\boldsymbol{k}} - \mu)\, c^\dagger_{\boldsymbol{k}\sigma} c_{\boldsymbol{k}\sigma}$, the free Green function $G^{(0)}_{\boldsymbol{k}\sigma}(\omega)$ and the free density of states $\rho(\varepsilon)$ are obtained as

$$G^{(0)}_{\boldsymbol{k}\sigma}(\omega) = \frac{1}{\omega + \mu - \varepsilon_{\boldsymbol{k}}}, \tag{19}$$

$$\rho(\omega) = A^{(0)}_\sigma(\omega) = \frac{1}{L}\sum_{\boldsymbol{k}} \delta(\omega - \varepsilon_{\boldsymbol{k}})\,. \tag{20}$$

For interacting systems the self-energy $\Sigma_{\boldsymbol{k}}(\omega)$ is defined as the difference between free and interacting reciprocal Green functions:

$$G_{\boldsymbol{k}\sigma}(\omega)^{-1} = G^{(0)}_{\boldsymbol{k}\sigma}(\omega)^{-1} - \Sigma_{\boldsymbol{k}\sigma}(\omega)\,, \tag{21a}$$

$$G_{\boldsymbol{k}\sigma}(\omega) = \frac{1}{\omega + \mu - \varepsilon_{\boldsymbol{k}} - \Sigma_{\boldsymbol{k}\sigma}(\omega)}\,. \tag{21b}$$

For a translationally invariant system the Green function and self-energy are diagonal in momentum space. It can also be useful instead to use a matrix notation in site indices, $G_{ij\sigma}(i\omega_n) = (\boldsymbol{G})_{ij,\sigma,n}$ etc., for which

$$\boldsymbol{G}^{-1} = \boldsymbol{G}^{(0)-1} - \boldsymbol{\Sigma}\,, \tag{22a}$$

$$\boldsymbol{G} = \boldsymbol{G}^{(0)} + \boldsymbol{G}^{(0)}\boldsymbol{\Sigma}\,\boldsymbol{G}\,. \tag{22b}$$

Eq. (21) or (22) are referred to as the (lattice) Dyson equation.
Without interactions, single-particle excitations simply correspond to the creation or removal of a particle in an eigenstate of H_0, and as such they propagate freely through the lattice. This perfectly sharp excitation occurs as a δ-function in the free spectral function (omitting spin indices for now),

$$A^{(0)}_{\boldsymbol{k}}(\omega) = \delta(\omega + \mu - \varepsilon_{\boldsymbol{k}})\,. \tag{23}$$

The situation in a many-body system with interactions is different: adding a particle or hole to an eigenstate does not give an eigenstate again, but rather a massive superposition of eigenstates. As a consequence, particle or hole excitations will usually be damped and have a finite lifetime. This is encoded in the complex (retarded) self-energy $\Sigma_{\boldsymbol{k}}(\omega)$, in terms of which the spectral function becomes

$$A_{\boldsymbol{k}}(\omega) = \frac{1}{\pi}\frac{\operatorname{Im}\Sigma_{\boldsymbol{k}}(\omega)}{(\omega + \mu - \varepsilon_{\boldsymbol{k}} - \operatorname{Re}\Sigma_{\boldsymbol{k}}(\omega))^2 + (\operatorname{Im}\Sigma_{\boldsymbol{k}}(\omega))^2}\,. \tag{24}$$

This reduces to a δ-function only if $\operatorname{Im}\Sigma_{\boldsymbol{k}}(\omega) \to 0^-$. On the other hand, if $\operatorname{Im}\Sigma_{\boldsymbol{k}}(\omega)$ is finite and not too large, the maxima of $A_{\boldsymbol{k}}(\omega)$ are located approximately at the zeros $\omega = E_{\boldsymbol{k}}$ of

$$\omega + \mu - \varepsilon_{\boldsymbol{k}} - \operatorname{Re}\Sigma_{\boldsymbol{k}}(\omega) = 0\,. \tag{25}$$

In the vicinity of $E_{\boldsymbol{k}}$ the Green function can then be approximated to lowest order as

$$G_{\boldsymbol{k}}(\omega) = \frac{Z_{\boldsymbol{k}}(E_{\boldsymbol{k}})}{\omega - E_{\boldsymbol{k}} + i\tau_{\boldsymbol{k}}(E_{\boldsymbol{k}})^{-1}}\,, \tag{26a}$$

$$Z_{\boldsymbol{k}}(\omega) = \quad [1 - \operatorname{Re}\Sigma_{\boldsymbol{k}}(\omega)]^{-1}\,, \tag{26b}$$

$$\tau_{\boldsymbol{k}}(\omega) = [-Z_{\boldsymbol{k}}(\omega)\operatorname{Im}\Sigma_{\boldsymbol{k}}(\omega)]^{-1}\,, \tag{26c}$$

where $Z_{\boldsymbol{k}}$ and $\tau_{\boldsymbol{k}}$ play the role of a quasiparticle weight and lifetime. In analogy to the non-interacting case, the maxima $E_{\boldsymbol{k}}$ of $A_{\boldsymbol{k}}(\omega)$ yield the *electronic dispersion*, i.e., the relation between crystal momentum and excitation energy, although this maximum may be quite broad.

A reliable quasiparticle picture is guaranteed in a Landau Fermi liquid close to the Fermi surface, i.e., near $\omega = 0$, because then $\mathrm{Re}\,\Sigma_{\boldsymbol{k}}(\omega)$ is linear and $\mathrm{Im}\,\Sigma_{\boldsymbol{k}}(\omega)$ quadratic in ω for small frequencies at zero temperature. Near $\omega = 0$ this leads to

$$E_{\boldsymbol{k}} = Z_{\boldsymbol{k}}(0)\big(\varepsilon_{\boldsymbol{k}} - \mu + \mathrm{Re}\,\Sigma_{\boldsymbol{k}}(0)\big)\,, \tag{27}$$

i.e., a linear relation between non-interacting and interacting dispersion. However angle-resolved photoemission (ARPES) nowadays provides a means to measure $A_{\boldsymbol{k}}(\omega)$ (times the Fermi function) even deep below the Fermi energy with high accuracy (see, e.g., Ref. [19]). Therefore the resonances given by (25) are relevant even if these excitations are not as coherent as low-energy excitations near the Fermi surface in a Landau Fermi liquid.

3.2 Hubbard bands and the Mott transition

Let us consider the atomic limit of the Hubbard model, i.e., no hopping, $t_{ij} = 0$. The Green function then becomes momentum-independent and reads

$$G^{\mathrm{at}}_{\boldsymbol{k}\sigma}(\omega) = \frac{n_{-\sigma}}{\omega + \mu - U} + \frac{1 - n_{-\sigma}}{\omega + \mu}\,, \tag{28}$$

which corresponds to a spectral function with two δ-peaks separated by an energy U, and the system is *insulating*, as there is no hopping at all. Next let us consider the situation for small hopping t_{ij}. Compared to the atomic limit the δ-peaks in the spectral function will broaden, i.e., two subbands develop, the *Hubbard bands*. The nature of these subbands is quite different from that of one-electron bands in non-interacting systems. For example, the upper Hubbard band describes charge excitations on top of the filled lower Hubbard band. If the hopping is increased further, or the Hubbard interaction U decreased, these Hubbard bands will eventually overlap and the system will become metallic at a critical value U_c on the order of the bandwidth. This correlation-induced *metal-insulator transition* does not break translational invariance and is called the Mott transition [20].

When starting from the atomic limit, a standard but unreliable method to capture the Mott metal-insulator transition is the so-called Hubbard-I approximation. Here one uses the atomic self-energy, obtained from (28),

$$\Sigma^{\mathrm{at}}_{\boldsymbol{k}\sigma}(\omega) = U n_{-\sigma} + U^2 \frac{n_{-\sigma}(1 - n_{-\sigma})}{\omega + \mu - U(1 - n_{-\sigma})}\,, \tag{29}$$

in the Dyson equation (21), which provides the Green function. However, this ad-hoc approximation exhibits several unphysical properties (discussed, e.g., in Ref. [21]). Starting from the weak-coupling side, a simple, rough picture of the Mott transition is provided by the Gutzwiller wave function (see [22] for a review), which describes a Mott insulator at half-filling when U becomes so large that all doubly occupied sites are projected out: this is the so-called Brinkman-Rice transition. These approximate understandings are quantitatively rathe inaccurate. Indeed, one of the successes of DMFT has been its description of the Mott metal-insulator transition in the infinite-dimensional Hubbard model, as discussed in Sec. 4.4 below.

3.3 Diagrammatic perturbation theory

The self-energy, according to (22), represents the contribution to the (inverse) Green function which is due to interactions. The perturbation theory for these quantities can be organized effectively into Feynman diagrams as follows [16–18].

Feynman diagrams for single-particle Green functions (for arbitrary quadratic H_0 and two-particle interaction H_1) are built from the following pieces:

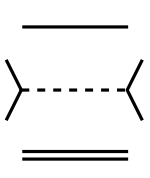

$= \text{non-interacting Green function line } \boldsymbol{G}^{(0)},$ (30a)

$= \text{interaction vertex},$ (30b)

$= \text{full (interacting) Green function line } \boldsymbol{G}\,.$ (30c)

The perturbation expansion in H_1 then produces a series of diagrams (unlabeled [17], and arrows omitted throughout) for the Green function

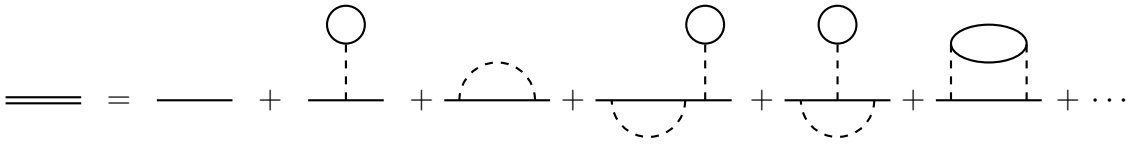

(31)

We will not review the diagrammatic rules here, but we note that each Green function line comes with a Matsubara frequency (or imaginary time) argument and a momentum (or site) argument, energy and momentum conservation holds at the interaction vertices, all variables of internal lines are integrated over, while the variables of external lines are held fixed.

Since some parts of the diagrams are repeating, one defines so-called proper self-energy diagrams, which are "one-particle irreducible" (i.e., cannot be cut in two pieces by cutting a single solid line) and have their external vertices amputated, which means that the non-interacting Green functions, which would normally be connected to external vertices, are omitted (because they already occur in other parts of the diagram). Some examples are:

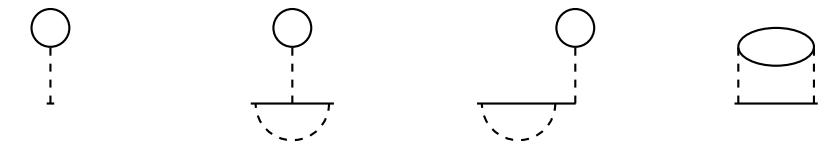

proper proper not proper proper (32)

The Dyson equation (21) can be expressed with Feynman diagrams as

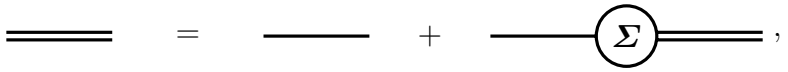

(33)

where the self-energy now has the following expansion,

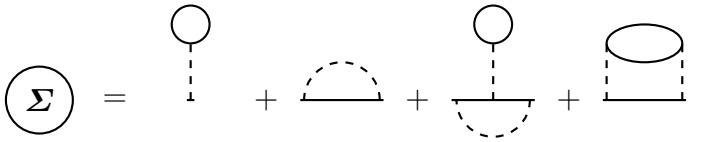

(34)

which, combined with (33), recovers (30).
This perturbation series for the self-energy has so far been written in terms of free Green functions, i.e., $\boldsymbol{\Sigma}$ depends on the function $\boldsymbol{G}^{(0)}$ in the sense that the whole matrix $\boldsymbol{G}^{(0)}(i\omega_n)$ for all frequency arguments enters into $\boldsymbol{\Sigma}$. In other words, $\boldsymbol{\Sigma} = \boldsymbol{\Sigma}[\boldsymbol{G}^{(0)}]$ is a *functional* of $\boldsymbol{G}^{(0)}$. The diagrams for $\boldsymbol{\Sigma}[\boldsymbol{G}^{(0)}]$ still contain self-energy insertions in their internal lines, i.e., some internal parts of the diagrams repeat which have already been enumerated. One can thus proceed to construct the so-called *skeleton expansion* which instead uses full (interacting) Green function lines $\boldsymbol{G}$

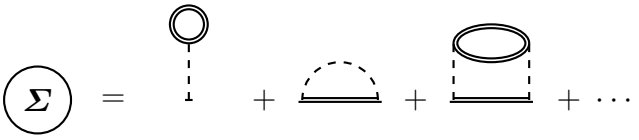

(35)

The diagrams in the skeleton expansion $\boldsymbol{\Sigma}[\boldsymbol{G}]$ no longer contain self-energy insertions on the Green function lines so that each self-energy diagram does not occur more than once.

3.4 Power counting in $1/d$

The consequences that the scaling in the limit $d \to \infty$ has for many-body theory [8, 23] is best discussed in terms of the Feynman diagrams for Green functions and the self-energy discussed above, in particular using the skeleton expansion.
We first consider the d dependence of $G_{ij\sigma}(\omega)$ in the limit $d \to \infty$, for scaled hopping amplitudes

$$t_{ij} = t^*_{ij}\, d^{-\frac{1}{2}||\boldsymbol{R}_i - \boldsymbol{R}_j||}\,. \tag{36}$$

Here $||\boldsymbol{R}_i - \boldsymbol{R}_j||$ is the fewest number of lattice steps that connect $\boldsymbol{R}_i$ to $\boldsymbol{R}_j$ on the hypercubic lattice, and hence proportional to the number of sites connected by the hopping amplitude t_{ij}, so that (36) has the correct scaling. By our construction the kinetic energy is finite in the limit $d \to \infty$, which can be expressed in terms of the Green function,

$$E_{\text{kin},\sigma} = \sum_{ij} t_{ij} \langle c^\dagger_{i\sigma} c_{j\sigma} \rangle = \sum_{ij} t_{ij} \int_{-\infty}^{\infty} \frac{d\omega}{2\pi i}\, G_{ij\sigma}(\omega)\, e^{i\omega 0^+} = \mathcal{O}(d^0)\,. \tag{37}$$

Here the double sum yields a contribution of order $Ld^{||\boldsymbol{R}_i - \boldsymbol{R}_j||}$. Hence we conclude

$$G_{ij\sigma}(\omega) = \mathcal{O}(d^{-\frac{1}{2}||\boldsymbol{R}_i - \boldsymbol{R}_j||})\,, \qquad\qquad G_{ii\sigma}(\omega) = \mathcal{O}(d^0)\,, \tag{38}$$

i.e., the off-diagonal Green function decays rapidly with distance, which leads to simplifications for the Feynman diagrams.

3.5 Local self-energy

For the discussion of the self-energy we will work with so-called Hugenholtz diagrams instead, which combine direct and exchange diagrams into a box vertex [17]. However, for the Hubbard interaction there are no exchange diagrams anyway. We thus replace

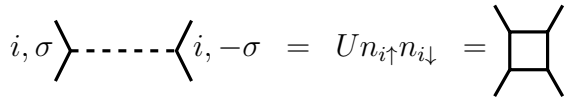

(39)

again omitting the arrows on the diagrams. We can then write the skeleton expansion as

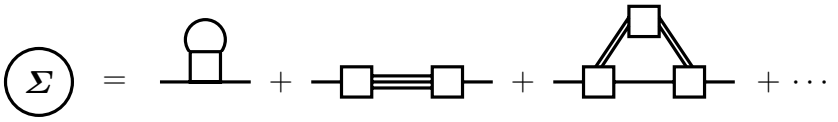

(40)

The skeleton expansion has the property that any two vertices are joined through Green function lines via at least three independent paths. Namely, suppose there is only one such path; then the diagram is one-particle irreducible, a contradiction. If there are only two paths, then they must run through a diagram part which is a self-energy insertion, which is also a contradiction.
Now consider an arbitrary diagram (in position space, so that the interaction vertices are labeled by lattice site vectors), in which two internal vertices labeled by i and j appear,

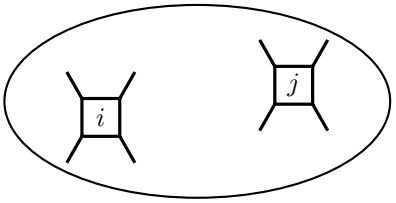

(41)

Let us hold i fixed for the moment. We now compare the case $j \neq i$ with the case $j = i$. Suppose $j \neq i$. As discussed above, there are three independent paths from the vertex i to the vertex j. The Green function lines on these paths can thus contribute at most $\mathcal{O}(d^{-\frac{3}{2}||\boldsymbol{R}_i - \boldsymbol{R}_j||})$ (or even less if there is another intermediate site $\boldsymbol{R}_k$ on a path). Although the summation over j contributes a factor of order $\mathcal{O}(d^{||\boldsymbol{R}_i - \boldsymbol{R}_j||})$, on the whole, any skeleton diagram is thus suppressed at least by a factor $\mathcal{O}(d^{-\frac{1}{2}||\boldsymbol{R}_i - \boldsymbol{R}_j||})$. As an example, consider

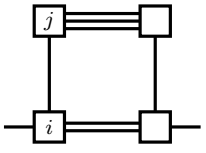

(42)

Even if the boxes without labels correspond to site j, there are three lines connecting i with j and only one summation over j.
By contrast, for $j = i$ the Green functions are of order $\mathcal{O}(d^0)$, and there is no summation. We thus conclude that only the case $i = j$ contributes in the limit $d \to \infty$, i.e., all diagrams in

the skeleton expansion $\boldsymbol{\Sigma}[\boldsymbol{G}]$ have the same lattice site label at all their internal and external vertices. Hence the self-energy is site-diagonal ("local"),

$$\Sigma_{ij\sigma}(\omega) = \delta_{ij}\ \Sigma_{ii\sigma}(\omega) = \delta_{ij}\ \Sigma_{\sigma}(\omega)\,, \tag{43}$$

or, equivalently, momentum-independent in $\boldsymbol{k}$ space,

$$\Sigma_{\boldsymbol{k}\sigma}(\omega) = \Sigma_{\sigma}(\omega)\,. \tag{44}$$

Furthermore, *the self-energy $\Sigma_\sigma(\omega)$ is a functional only of the local Green function $G_\sigma(\omega)$*, because all internal vertices in the skeleton expansion have the same site label.
The simple form of the self-energy has some immediate consequences also for the Green function (22), namely

$$G_{\boldsymbol{k}\sigma}(\omega) = \frac{1}{\omega + \mu - \varepsilon_{\boldsymbol{k}} - \Sigma_\sigma(\omega)} = G^{(0)}_{\boldsymbol{k}\sigma}\big(\omega - \Sigma_\sigma(\omega)\big)\,. \tag{45}$$

Summing over $\boldsymbol{k}$ gives us the local Green function as

$$G_\sigma(\omega) = \int \frac{d^dk}{(2\pi)^d} \frac{1}{\omega + \mu - \varepsilon_{\boldsymbol{k}} - \Sigma_\sigma(\omega)} \tag{46}$$

$$= \int_{-\infty}^{\infty} d\omega\ \frac{\rho(\varepsilon)}{\omega + \mu - \Sigma_\sigma(\omega) - \varepsilon}\,. \tag{47}$$

The last equation thus provides a relation between the local self-energy and the local Green function. It involves only the dispersion via the non-interacting density of states. This relation is one of the ingredients of DMFT, as discussed below.

4 Dynamical mean-field theory

As seen above, the self-energy becomes site-diagonal and thus momentum-independent in the limit $d \to \infty$. The last step is now to actually construct the functional $\Sigma_\sigma[G_\sigma]$ [1–3, 24, 25], which will complete the derivation of the DMFT equations.

4.1 Path-integral representation

Green functions for many-body systems may be represented in a path integral representation [17]. The partition function and the imaginary-time-ordered Green function for the fermionic Hamiltonian $H(\{c^\dagger_\alpha\}, \{c_\alpha\})$ can be written in terms of functional integrals over Grassmann variables

$$Z = \mathrm{Tr} e^{-\beta(H-\mu N)} = \int\limits_{\phi_\alpha(\beta)=-\phi_\alpha(0)} \mathcal{D}(\phi^*_\alpha(\tau), \phi_\alpha(\tau))\ \exp(\mathcal{A})\,, \tag{48}$$

$$G_{\alpha\beta}(\tau) = \frac{1}{Z} \int\limits_{\phi_\alpha(\beta)=-\phi_\alpha(0)} \mathcal{D}(\phi^*, \phi)\ \phi_\alpha(\tau)\phi^*_\beta(0)\ \exp(\mathcal{A})\,, \tag{49}$$

with the action

$$\mathcal{A} = -\int_0^\beta d\tau \left[\sum_\alpha \phi_\alpha^* \left(\partial_\tau - \mu\right) \phi_\alpha + H(\{\phi_\alpha^*\}, \{\phi_\alpha\}) \right] . \tag{50}$$

Note that the Grassmann fields $\phi_\alpha^*(\tau)$ and $\phi_\alpha(\tau)$ are independent (i.e., they are not complex or Hermitian conjugates of each other, even though they represent creation and annihilation operators) and antiperiodic boundary conditions are imposed on the latter. Path-integral expressions such as (49) and (50) are actually just abbreviations for limits of expressions that are discretized in imaginary time τ. We refer to Ref. [17] for details.

4.2 Mapping onto effective impurity models

It is now possible to construct an effective single-site action which matches that of the Hubbard model in infinite dimensions [24]. For this purpose let us consider an action, $\mathcal{A} = \mathcal{A}_1 + \mathcal{A}_2$, consisting of a quadratic part and an interaction, which only involves one lattice site

$$\mathcal{A}_1 = \int_0^\beta d\tau \int_0^\beta d\tau' \sum_\sigma c_\sigma^*(\tau)\, \mathcal{G}_\sigma^{-1}(\tau,\tau')\, c_\sigma(\tau') = \sum_{n,\sigma} c_\sigma^*(i\omega_n)\, \mathcal{G}_\sigma(i\omega_n)^{-1}\, c_\sigma(i\omega_n), \tag{51a}$$

$$\mathcal{A}_2 = -U \int_0^\beta d\tau\; c_\uparrow^*(\tau) c_\uparrow(\tau) c_\downarrow^*(\tau) c_\downarrow(\tau), \tag{51b}$$

with some as yet unfixed "free" Green function $(\boldsymbol{\mathcal{G}}^{-1})_{\tau,\tau'} = \mathcal{G}_\sigma^{-1}(\tau,\tau')$, which also depends only on imaginary-time differences.

We can calculate the imaginary-time-ordered Green function of the single degree of freedom c from the action (51), and Fourier transform to Matsubara frequencies. This is abbreviated as

$$G_\sigma(i\omega_n) = \langle c_\sigma(i\omega_n) c_\sigma^*(i\omega_n) \rangle_{\mathcal{A}[\mathcal{G}]} . \tag{52}$$

Correspondingly, we define the impurity *impurity self-energy* $\widetilde{\boldsymbol{\Sigma}}$ via the *impurity Dyson equation*,

$$\boldsymbol{G} = \left[\boldsymbol{\mathcal{G}}^{-1} - \widetilde{\boldsymbol{\Sigma}} \right]^{-1} . \tag{53}$$

Now consider the diagrams in the skeleton expansion of $\widetilde{\boldsymbol{\Sigma}}[\boldsymbol{G}]$,

$\widetilde{\boldsymbol{\Sigma}}[\boldsymbol{G}] \;=$ 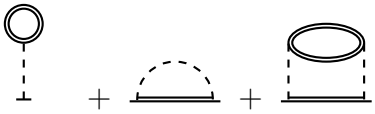 $+ \cdots ,$ (54)

in which of course only the single site of (51) occurs. However, since the local Hubbard interaction is the same both for the lattice Hubbard model and the single-site action, this skeleton expansion is exactly the same as that for the Hubbard model (35), i.e.,

$$\widetilde{\boldsymbol{\Sigma}}[\boldsymbol{G}] = \boldsymbol{\Sigma}[\boldsymbol{G}] . \tag{55}$$

This shows that the self-energy skeleton functional $\Sigma_\sigma[G_\sigma]$ can be obtained by solving the single-site problem (51). In the next section we discuss how to choose $\mathcal{G}_\sigma$ appropriately.

4.3 Dynamical mean-field equations

Putting everything together, we arrive at three DMFT equations, which determine three unknowns: the local Green function $G_\sigma(i\omega_n)$, the *dynamical mean field* (or *Weiss field*) $\mathcal{G}_\sigma(i\omega_n)$, and the local self-energy $\Sigma_\sigma(i\omega_n)$:

$$G_\sigma(i\omega_n) = \langle c_\sigma(i\omega_n) c_\sigma^*(i\omega_n) \rangle_{\mathcal{A}[\mathcal{G}]}, \tag{DMFT-1}$$

$$G_\sigma(i\omega_n) = \left[\mathcal{G}_\sigma(i\omega_n)^{-1} - \Sigma_\sigma(i\omega_n) \right]^{-1}, \tag{DMFT-2}$$

$$G_\sigma(i\omega_n) = \int d\varepsilon \, \frac{\rho(\varepsilon)}{i\omega_n + \mu - \Sigma_\sigma(i\omega_n) - \varepsilon}. \tag{DMFT-3}$$

Note that the *self-consistency equation* (47) provides precisely the needed relation (DMFT-3) to fix the Weiss field $\mathcal{G}_\sigma$. This ensures that one solves the correct single-site problem, i.e., the one which corresponds to the Hubbard model on a lattice with density of states $\rho(\varepsilon)$.

A typical iterative solution then proceeds a follows: Start with some Weiss field $\mathcal{G}_\sigma$, obtain G_σ from (DMFT-1), determine Σ_σ from the impurity Dyson equation (DMFT-2), calculate G_σ from the self-consistency equation (DMFT-3), obtain $\mathcal{G}_\sigma$ by using (DMFT-2) again, and repeat until convergence is reached.

One can check that the DMFT equations reproduce the correct non-interacting and atomic limits. (i) In the non-interacting case we have $U = 0$ and thus $\Sigma_\sigma(i\omega_n) = 0$. Furthermore it follows from (DMFT-3) that then $G_\sigma(i\omega_n) = G_\sigma^{(0)}(i\omega_n)$. Finally (DMFT-2) gives $\mathcal{G}_\sigma(i\omega_n) = G_\sigma(i\omega_n)$, and this agrees with (DMFT-1) for $U = 0$. (ii) On the other hand, in the atomic limit we have $t_{ij} = 0$ and $\varepsilon_{\boldsymbol{k}} = 0$, i.e., $\rho(\varepsilon) = \delta(\varepsilon)$. From (DMFT-3) we obtain $G_\sigma(i\omega_n) = [i\omega_n + \mu - \Sigma_\sigma(i\omega_n)]^{-1}$, and (DMFT-2) yields $\mathcal{G}_\sigma(i\omega_n)^{-1} = i\omega_n + \mu$, i.e., $\mathcal{G}_\sigma^{-1}(\tau) = -\partial_\tau + \mu$, which agrees with (DMFT-1) for $t_{ij} = 0$.

For a given non-zero value of the Hubbard interaction U the Green function obtained from the local action (51) clearly represents the most difficult of the DMFT equations. To obtain the impurity Green function from it, a dynamical single-site problem must be solved, usually with numerical methods. For finite temperatures quantum and thermal averages this can be stochastically sampled with quantum Monte Carlo (QMC) methods. The older Hirsch-Fye QMC algorithm [25–27] uses a fixed imaginary time-grid, whereas the more effective continuous-time (CT) QMC [28–30] samples creation and annihilation of particles at arbitrary imaginary times. Methods that also work for zero temperature include exact diagonalization (ED) [31–33], the numerical renormalization group (NRG) [34, 35] and the density-matrix renormalization group (DMRG) [36, 37]. Several of these methods are discussed in the other lectures of this book. A number of perturbative or semianalytic methods is also available [1].

To use these "impurity solvers", the single-site action (51) is often not used directly, but rather an impurity problem defined by a Hamiltonian is considered, usually by constructing a single-impurity Anderson model (SIAM)

$$H_{\text{SIAM}} = \sum_{\ell\sigma} \varepsilon_\ell \, a_{\ell\sigma}^\dagger a_{\ell\sigma} + \sum_{\ell\sigma} V_\ell \left(a_{\ell\sigma}^\dagger c_\sigma + c_\sigma^\dagger a_{\ell\sigma} \right) + U \, c_\uparrow^\dagger c_\uparrow c_\downarrow^\dagger c_\downarrow \,. \tag{56}$$

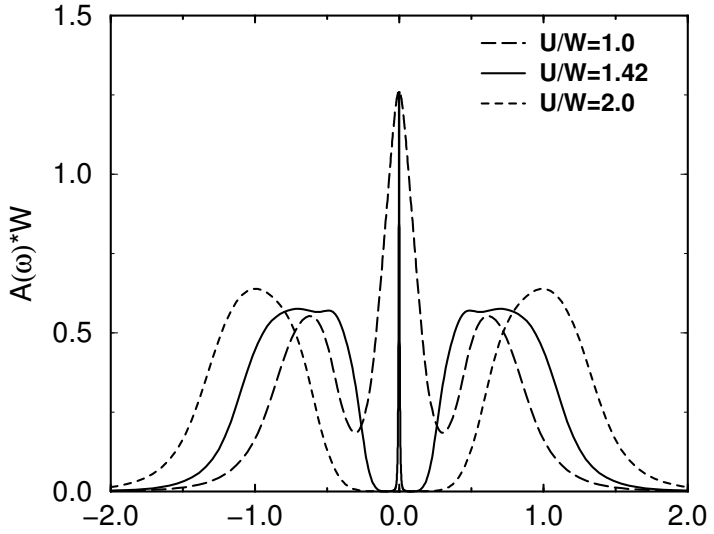

Fig. 2: *Zero-temperature spectral function for the homogeneous phase of the Hubbard model on the Bethe lattice with nearest-neighbor hopping and bandwidth $W = 4|t_*|$ at half-filling, evaluated with NRG. From Ref. [34].*

Here the fermions $a_{\ell\sigma}$ represent a non-interacting bath which hosts the interacting fermion c_σ. This bath can be at once integrated out from the action which represents H_{SIAM}, because this involves only Gaussian (path) integrals. The resulting action is then precisely of the form (51), with

$$\mathcal{G}_\sigma^{-1}(i\omega_n) = i\omega_n + \mu - \frac{1}{\pi}\int_{-\infty}^{\infty} d\omega\, \frac{\Delta(\omega)}{i\omega_n - \omega}\,, \qquad \Delta(\omega) = \pi \sum_\ell V_\ell^2\, \delta(\omega - \varepsilon_\ell)\,, \tag{57}$$

where $\Delta(\omega)$ is called the hybridization function. In the DMFT iteration cycle one must now find the parameters V_ℓ and ε_ℓ that allow a self-consistent DMFT solution. Then the SIAM has been determined which properly represents the infinite-dimensional Hubbard model in DMFT. For reference we note that the self-consistency equation (DMFT-3) yields a simple relation for nearest-neighbor hopping t_* on the Bethe lattice with density of states (9),

$$\mathcal{G}_\sigma(i\omega_n) = i\omega_n + \mu - t_*^2 G(i\omega_n)\,. \tag{58}$$

This relation and generalizations for other types of hopping are discussed in Refs. [1, 10, 11, 14, 15].

4.4 Results for the Hubbard model

Some aspects of the spectrum and the DMFT phase diagram of the Hubbard model were discussed already in the Lecture of D. Vollhardt. Fig. 2 shows the zero-temperature spectral function for the homogeneous phase of the Hubbard model on the Bethe lattice with nearest-neighbor hopping and bandwidth $W = 4|t_*|$ at half-filling, evaluated with NRG. Three values of U are shown, one in the metallic phase (three peaks in the spectral function), one close to the critical value U_c, and one for the insulating phase (with gap in the spectral function). At the

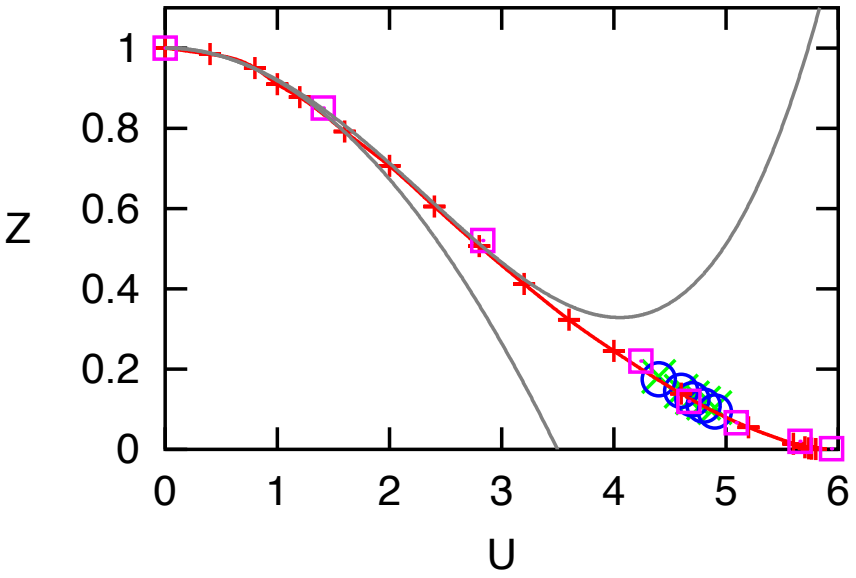

Fig. 3: *Quasiparticle weight Z for the half-filled Hubbard model on the Bethe lattice (with $t_* = 1$) in DMFT. Crosses $+$: NRG; squares: ED; crosses $\times$ and circles: QMC extrapolations; lower gray line: 2nd order perturbation theory in U, upper gray line: 4th order perturbation theory in U. From Ref. [10].*

Fermi energy the spectral function has the same value for all U in the metallic phase; this is a consequence of Luttinger's theorem [8]. In the metallic phase the weight of the central peak is proportional to the Fermi liquid quasiparticle renormalization factor Z (see (27)), whereas the outer two peaks are the developing Hubbard bands. Note that the energy resolution of NRG is best near the Fermi surface, i.e., near $\omega = 0$. Higher-resolution DMRG calculations have shown that there is actually a more pronounced substructure at the inner edges of the Hubbard bands close to U_c [36, 37], which has been attributed to the effective interaction of so-called doublon-holon pairs [38].

Fig. 3 shows the renormalization factor Z in the limit of zero temperature obtained with various methods. It starts from $Z = 1$ for the non-interacting case and decreases as U is increased, corresponding to the decreasing width of the central peak in the spectral function and an increasingly flatter dispersion. At U_c, the half-filled system undergoes a Mott metal insulator transition, i.e., it becomes localized and Z vanishes accordingly.

4.5 Results for the Falicov-Kimball model

The Falicov-Kimball model is a simplified version of the Hubbard model, in which only one of the two spin species is mobile (relabeled as d_i), while the other (relabeled as f_i) is not. For this model the Green function can be derived explicitly from the DMFT action [39]; higher-order Green functions can also be obtained [40, 41]. The Hamiltonian reads

$$H = \sum_{ij} t_{ij}\, d_i^\dagger d_j + E_f \sum_i f_i^\dagger f_i + U \sum_i d_i^\dagger d_i f_i^\dagger f_i \,, \tag{59}$$

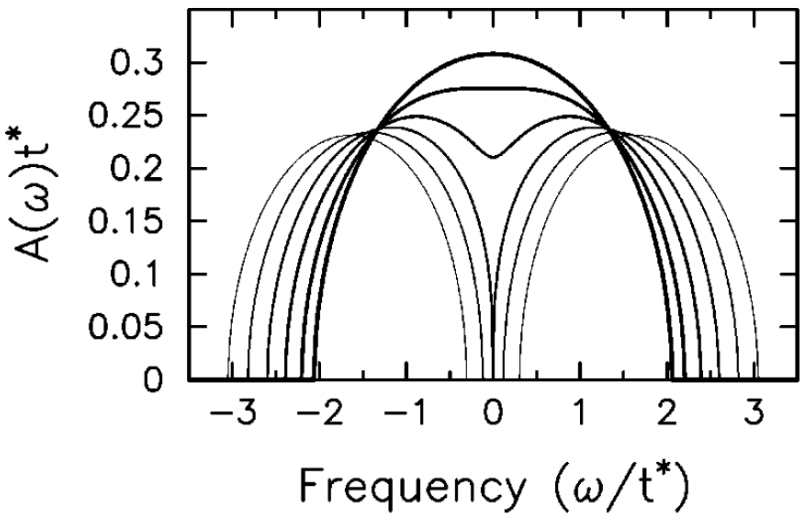

Fig. 4: *Spectral function of itinerant d electrons for the Falicov-Kimball model in DMFT for nearest-neighbor hopping on the Bethe lattice, homogeneous phase, $n_d = n_f = 1/2$, and $U = 0.5, 1.0, \ldots 3.0$. From Ref. [39].*

i.e., the d electrons are moving against a background of static f electrons, whose configuration is chosen such that it optimizes the free energy. In principle this makes the model quite complicated, as one needs the spectrum of H for all the possible f configurations. In dimensions $d \geq 2$ it is known that at half-filling on a bipartite lattice checkerboard order of the f electrons appears in the ground state and persists up to a finite critical temperature [42]. Here we consider only the homogeneous phase in DMFT for simplicity.

Since there is no hopping amplitude for the f electrons, the DMFT self-consistency yields at once $\mathcal{G}_f^{-1} = -\partial_\tau + \mu + E_f$, as explained above for the atomic limit. The DMFT action is thus given by

$$\begin{aligned}\mathcal{A} = &\int_0^\beta d\tau \int_0^\beta d\tau' d^*(\tau)\, \mathcal{G}_d^{-1}(\tau,\tau')\, d(\tau') \\ &+ \int_0^\beta d\tau f^*(\tau)(\partial_\tau - \mu + E_f)\, f(\tau) - U \int_0^\beta d\tau\; d^*(\tau)d(\tau)f^*(\tau)f(\tau). \end{aligned} \tag{60}$$

Now the f electrons can be integrated out at each lattice site, i.e., they are in the atomic limit (cf. Sec. 3.2). This leads to

$$G_d(i\omega_n) = \langle d(i\omega_n) d^*(i\omega_n)\rangle_{\mathcal{A}} = \frac{n_f}{\mathcal{G}_d(i\omega_n)^{-1} - U} + \frac{1-n_f}{\mathcal{G}_d(i\omega_n)^{-1}}\,, \tag{61}$$

which must be solved together with the other two DMFT equations

$$G_d(i\omega_n) = \int_{-\infty}^{\infty} \frac{d\varepsilon\; \rho_d(\varepsilon)}{i\omega_n + \mu - \Sigma_d(i\omega_n) - \varepsilon}\,, \tag{62}$$

$$G_d(i\omega_n)^{-1} = \mathcal{G}_d(i\omega_n)^{-1} - \Sigma_d(i\omega_n)\,. \tag{63}$$

This set of equations determines the d-electron Green function $G_d(i\omega_n)$ for any density of states $\rho_d(\varepsilon)$. Analytic continuation to real frequencies shows at once that the spectra in the homogeneous phase are independent of temperature. Note that this no longer holds in the checkerboard phase). Fig. 4 shows the spectral function $A_d(\omega)$ for several U for the Bethe lattice (with nearest-neighbor hopping $t_* = 1$). In particular there is a Mott metal-insulator transition taking place at $U_c = 2$; for larger U a band gap develops. Nevertheless, the transition is qualitatively different from that in the Hubbard model. For example, for the Falicov-Kimball model it can be shown from the low-energy form of the self-energy that for $0 < U < U_c$ the metallic state is not a Landau Fermi liquid; as a consequence, the spectral function is not pinned at the Fermi surface.

It is also possible to solve for the d self-energy as a functional of the d Green function, i.e., for the skeleton expansion $\Sigma_d[G_d]$ [21]

$$\Sigma_d(i\omega_n) = \frac{U}{2} - \frac{1}{2G_d(i\omega_n)} \pm \sqrt{\left(\frac{U}{2} - \frac{1}{2G_d(i\omega_n)}\right)^2 + \frac{Un_f}{G_d(i\omega_n)}}\,, \tag{64}$$

which is independent of the density of states $\rho(\varepsilon)$. Note that in contrast to the Hubbard model, for the Falicov-Kimball model the skeleton functional is in fact only a *function* of the Green function, i.e., $\Sigma_d(i\omega_n)$ depends only on $G_d(i\omega_n)$ at the same Matsubara frequency.

5 Summary and outlook

In this lecture we reviewed the foundations of dynamical mean-field theory for the infinite-dimensional single-band Hubbard model, i.e., the scaling of hopping amplitudes, the local nature of the self-energy, and the mapping onto a dynamical single-site problem in an effective bath which has to be determined self-consistently. Some of the numerical approaches to the effective single-site problem, also for the multiband case, are discussed in the other lectures in this school. Also, important generalizations beyond single-site DMFT to clusters and beyond local self-energies are discussed there, which are important for the accurate description of in fact finite-dimensional systems. DMFT therefore leads not only to nonperturbative numerical solutions to Hubbard-type models in infinite dimensions, but it is also a robust starting point for approximate theories of finite-dimensional systems.

Acknowledgment

Support of the Deutsche Forschungsgemeinschaft through the former FOR 1346 and TRR 80 is gratefully acknowledged.

References

[1] A. Georges, G. Kotliar, W. Krauth, and M.J. Rozenberg, Rev. Mod. Phys. **68**, 13 (1996)

[2] D. Vollhardt: *Investigations of correlated electron systems using the limit of high dimensions* in: V.J. Emery (ed.): *Correlated Electron Systems* (World Scientific, 1993)

[3] D. Vollhardt in A. Avella, F. Mancini (eds.): *Lectures on the Physics of Strongly Correlated Systems XIV*, AIP Conference Proceedings Vol. 1297 (American Institute of Physics, Melville, 2010), p. 339; arXiv:1004.5069

[4] D. Vollhardt, K. Byczuk, and M. Kollar: *Dynamical Mean-Field Theory*, in: A. Avella and F. Mancini (eds.): *Theoretical Methods for Strongly Correlated Systems* (Springer, 2011)

[5] A. Georges: *Dynamical Mean-Field Theory: Materials from an Atomic Viewpoint beyond the Landau Paradigm* in: E. Pavarini, E. Koch, D. Vollhardt, and A. Lichtenstein (eds.): *DMFT at 25: Infinite Dimensions*, Modeling and Simulation Vol. 4 (FZ Jülich, 2011)

[6] M. Kollar: *Introduction to Dynamical Mean-Field Theory* in: E. Pavarini, E. Koch, A. Lichtenstein, and D. Vollhardt (eds.), *The LDA+DMFT approach to strongly correlated materials*, Modeling and Simulation Vol. 1 (Forschungszentrum Jülich, 2011)

[7] W. Metzner and D. Vollhardt, Phys. Rev. Lett. **62**, 324 (1989)

[8] E. Müller-Hartmann, Z. Phys. B **74**, 507 (1989)

[9] J. Schlipf, Ph.D. Thesis, Universität Augsburg (1998)

[10] N. Blümer, *Metal-Insulator Transition and Optical Conductivity in High Dimensions* (Shaker Verlag, Aachen, 2003)

[11] N. Blümer and P.G.J. van Dongen: *Transport properties of correlated electrons in high dimensions* in A.C. Hewson and V. Zlatic (eds.): *Concepts in Electron Correlation* (Kluwer, 2003); arXiv:cond-mat/0303204

[12] E. Müller-Hartmann, in E. Talik and J. Szade (eds.): *Proceedings of the V. Symposium "Physics of Metals"* (Ustroń, 1991)

[13] G. Santoro, M. Airoldi, S. Sorella, and E. Tosatti, Phys. Rev. B **47**, 16216 (1993)

[14] M. Eckstein, M. Kollar, K. Byczuk and D. Vollhardt, Phys. Rev. B **71**, 235119 (2005)

[15] M. Kollar, M. Eckstein, K. Byczuk, N. Blümer, P. van Dongen, M.H. Radke de Cuba, W. Metzner, D. Tanaskovic, V. Dobrosavljevic, G. Kotliar, and D. Vollhardt, Ann. Phys. (Leipzig) **14**, 642 (2005)

[16] A.L. Fetter and J.D. Walecka: *Quantum Theory of Many-Particle Systems* (McGraw-Hill, 1971)

[17] J.W. Negele and H. Orland: *Quantum Many-Particle Systems* (Addison-Wesley, 1988)

[18] R.D. Mattuck, *A Guide to Feynman Diagrams in the Many-Body Problem*, 2nd Edition (Dover Publications, 1992)

[19] X.J. Zhou, T. Cuk, T. Devereaux, N. Nagaosa, and Z.-X. Shen in J.R. Schrieffer (ed.): *Handbook of High-Temperature Superconductivity: Theory and Experiment* (Springer, 2007), p. 87; arXiv:cond-mat/0604284

[20] N.F. Mott, Proc. Phys. Soc. A (London) **62**, 416 (1947)

[21] F. Gebhard, *The Mott Metal-Insulator Transition* (Springer, Berlin, 1997)

[22] D. Vollhardt, Rev. Mod. Phys. **56**, 99 (1984)

[23] E. Müller-Hartmann, Z. Phys. B **76**, 211 (1989)

[24] A. Georges and G. Kotliar, Phys. Rev. B **45**, 6479 (1992)

[25] M. Jarrell, Phys. Rev. Lett. **69**, 168 (1992)

[26] M.J. Rozenberg, X.Y. Zhang, and G. Kotliar, Phys. Rev. Lett. **69**, 1236 (1992)

[27] A. Georges and W. Krauth, Phys. Rev. Lett. **69**, 1240 (1992)

[28] A.N. Rubtsov, V.V. Savkin, and A.I. Lichtenstein, Phys. Rev. B **72**, 035122 (2005)

[29] P. Werner, A. Comanac, L. de' Medici, M. Troyer, and A.J. Millis, Phys. Rev. Lett. **97**, 076405 (2006)

[30] K. Haule, Phys. Rev. B **75**, 155113 (2007)

[31] M. Caffarel and W. Krauth, Phys. Rev. Lett. **72**, 1545 (1994)

[32] Q. Si, M.J. Rozenberg, G. Kotliar, and A.E. Ruckenstein, Phys. Rev. Lett. **72**, 2761 (1994)

[33] M.J. Rozenberg, G. Moeller, and G. Kotliar, Mod. Phys. Lett. B **8**, 535 (1994)

[34] R. Bulla, Phys. Rev. Lett. **83**, 136 (1999)

[35] R. Bulla, T.A. Costi, and Th. Pruschke, Rev. Mod. Phys. **80**, 395 (2008)

[36] D.J. García, K. Hallberg, and M.J. Rozenberg, Phys. Rev. Lett. **93**, 246403 (2004)

[37] M. Karski, C. Raas, and G.S. Uhrig, Phys. Rev. B **77**, 075116 (2008)

[38] S.-S.B. Lee, J. van Delft, and A. Weichselbaum, Phys. Rev. Lett. **119**, 236402 (2017)

[39] J.K. Freericks and V. Zlatić, Rev. Mod. Phys. **75**, 1333 (2003)

[40] T. Ribic, G. Rohringer, K. Held, Phys. Rev. B **93** 195105 (2016)

[41] T. Ribic, G. Rohringer, K. Held, Phys. Rev. B **95** 155130 (2017)

[42] T. Kennedy and E.H. Lieb, Physica A **138** 320 (1986)